

# Development of Cable-driven Anthropomorphic Robot Hand\*

Sungjae Min and Sooyeong Yi

**Abstract**—This letter presents a novel design of an anthropomorphic robotic hand. By using a parallel plate knuckle with a universal joint, it is possible to achieve two degree of freedom (DOF) at a joint of a finger with wide working range in the proposed design. Each degree of freedom of the robotic hand is driven by parallel cables with single motor that mimics the muscle antagonism of the human hand. The proposed robotic hand embodies human-like features and achieves an adaptive grasping capability by adopting compliant coupling between the distal and the proximal interphalangeal joints. Experiments are conducted to validate the performance of the robotic hand.

**Index Terms**—Actuation and joint mechanisms, grippers and other end-effectors, multifingered hands, parallel robots, Tendon/wire mechanism.

## I. INTRODUCTION

THE human hand is one of the most sophisticated organs. It is light, strong, and has a high degree of freedom (DOF) because of being composed of several bones, tendons, and muscles, thus demonstrates a high level of dexterity in performing various tasks. It enables human interaction with the environment by allowing us to touch and grasp objects around us [1], [2], [3].

Recent advancement in studies on human–robot interaction and assistive robots has led to an increasing interest in the concept of a robotic hand. A robotic hand serves two main purposes: (1) medical, that is, as the prosthesis of amputees, and (2) industrial, that is, as a multifunctional tool for robot manipulators. Several research projects have reportedly designed a robotic hand by mimicking the functionality of a human hand [4], [5].

It is difficult to realize a light and strong anthropomorphic robotic hand because it is challenging to fit many actuators and sensors into a compact structure [2], [6]. To overcome this challenge, a conventional robotic hand is generally designed with fixed mechanical linkage between joints of a finger or with only three or four fingers at the cost of dexterity and DOF [2],

Manuscript received October 7, 2020; accepted January 12, 2021. Date of publication February 2, 2021; date of current version February 17, 2021. This letter was recommended for publication by Associate Editor D. Yang and Editor H. Liu upon evaluation of the reviewers' comments. This work was supported by the research program funded by the National Research Foundation (Ministry of Education) of Korea (NRF-2018R1D1A1B07044841). (Corresponding author: Sooyeong Yi.)

The authors are with the Department of Electrical and Information Engineering, Seoul National University of Science and Technology, Seoul 01811, Republic of Korea (e-mail: msj5826@gmail.com; suylee@seoultech.ac.kr).

\* A short video clip of the proposed robotic hand's motion can be found in <https://youtu.be/GzXvqFWgls4>.

Digital Object Identifier 10.1109/LRA.2021.3056375

[6]. For instance, the Sensor-Hand is a light prosthetic hand that has only one actuator and two fingers with coupled joints [7], [8]. The Michelangelo-Hand has its fingers linked together at a single point actuated by one motor [9]. Most of the robotic hands have a similar four-bar linkage at the proximal interphalangeal (PIP) and the distal interphalangeal (DIP) joints of a finger to enable a coupled motion between the joints [10], [11], [12]. Instead of the passive mechanical linkage between the joints, the four-fingered KITECH-Hand has independent motors deployed at each joint of a finger to improve dexterity [13]. Unlike the human hand, which has a yaw–pitch motion at the metacarpophalangeal (MCP) joint of a finger, the KITECH-Hand adopts a roll–pitch motion at the MCP joint. However, the motor deployed at each finger joint imposes a load on the motor at the previous joint. The recent studies have followed a biomimetic approach using tendons in order to deploy the motors aside the hand and achieve a light and strong anthropomorphic robotic hand.

In a biomimetic robotic hand, the ligaments and tendons of the human hand are replaced with elastic elements and cables, and the natural motion of the human hand is realized with the reduced number of actuators [4]. The similar biomimetic approaches for a cable-driven robotic arm and a cable-driven joint module are presented in [14], [15]. The DIST-Hand is a cable-driven, four-fingered, modularized robotic hand with four DOFs at each finger [16]. In [5], the anatomically correct testbed (ACT) hand is presented by mimicking the underlying mechanics and controls of the human hand using cables and motors instead of tendons and muscles. The historical progress and prospects of studies conducted on robotic hands are available in [2], [6].

This letter presents a novel design of a cable-driven anthropomorphic robotic hand shown in Fig. 1. In the figure, there are two versions of the test-bed hand and the hand with forearm. Two versions of the robotic hands are exactly same except the motor mount block. The main features of the robotic hand are the antagonistic actuation for a finger joint by parallel cables with a single motor and the compliant under-actuation between the PIP and the DIP joints with an extension spring. A parallel knuckle mechanism is proposed to conveniently achieve the antagonistic actuation in this study, that has two DOFs at a joint and wide working range with simple structure.

Owing to its cable-driven and under-actuated structure, it is possible to reduce the total number of motors and realize a light and strong robotic hand. In addition, because the proposed robotic hand uses off-the-shelf and 3D printable components only, it is simple and cost-effective to implement. Recent advancement in 3D-printing technology has resulted in

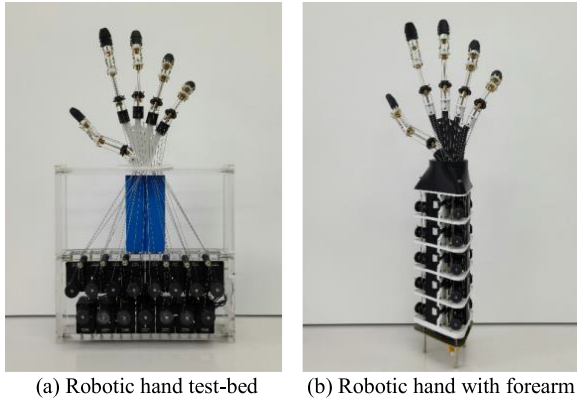


Fig. 1. Parallel cable-driven robotic hand.

TABLE I  
GENERAL CHARACTERISTICS OF THE ROBOTIC HAND

Weight (g)	No. of joints	Degree of freedom	No. of actuators
191	15	20	15

TABLE II  
KINEMATIC PARAMETERS OF THE ROBOTIC HAND

(a) Kinematic range of each joint (deg.)

Pitch at MCP( $\varphi_1$ )	Yaw at MCP( $\theta_1$ )	Pitch at PIP ( $\varphi_2$ )	Pitch at DIP ( $\varphi_3$ )
$ \varphi_1  +  \theta_1  \leq 60$	$0 \leq \varphi_2 \leq 90$	$0 \leq \varphi_3 \leq 90$	

(b) Phalange length (mm)

Finger	Link			
	Link0	Link1	Link2	Link3
Thumb	15.0	42.5	40.0	30.0
Index	15.0	42.5	27.5	25.0
Middle	15.0	47.5	27.5	25.0
Ring	15.0	45.0	27.5	25.0
Little	15.0	40.0	22.5	22.5

an increased interest in robotic hands that can be produced by simply using 3D printers [17]–[20]. The rest of this letter is organized as follows. In Section II, the general characteristics including the kinematic structure of the proposed robotic hand are presented. The features of the robotic hand are explained in detail in Section III. The joint actuation obtained by parallel cables and the compliant under-actuation between the joints are explained in Sections III.A and III.B, respectively. Section III.C describes the thumb disposition of the robotic hand to improve the opposability. Section IV presents the experimental results and Section V addresses the concluding remarks.

## II. CABLE-DRIVEN ROBOTIC HAND

Fig. 1 shows the proposed cable-driven robotic hand, whose general characteristics are presented in Tables I and II. The phalangeal length and kinematic range of each finger joint in Table II are designed with reference to those of the human hand.

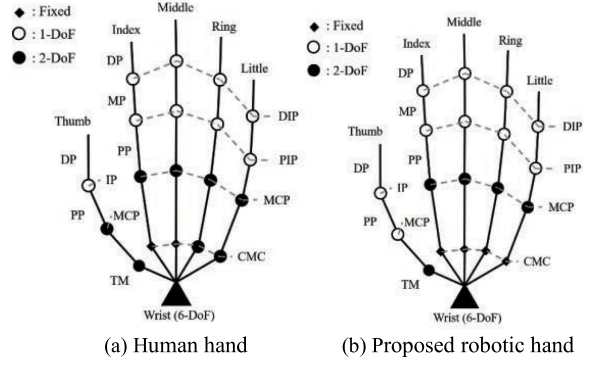


Fig. 2. Comparison between human hand and robotic hand.

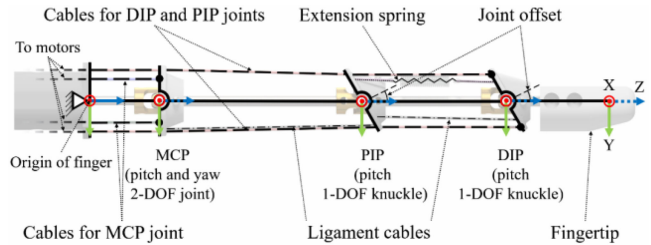


Fig. 3. Structure of a finger of the robotic hand.

The weight in Table I represents that of the robotic hand without motors. The total weight of the forearm model in Fig. 1 is 934 g.

Fig. 2 compares the DOFs at each joint between the human hand and the proposed robotic hand. All fingers of the proposed robotic hand have the same kinematic structure with different lengths. The kinematic structure of one finger is shown in Fig. 3. The MCP joint exhibits yaw–pitch motion actuated by four antagonistic cables and the DIP joint is driven by two cables to exhibit pitch motion. The PIP joint is coupled with the DIP joint by an extension spring. The yaw motion corresponds to the abduction–adduction and the pitch motion represents the flexion–extension of the human finger. Table III shows comparison of the proposed robotic hand with the other hands. A finger of the human hand has a ligament that limits a joint motion beyond a certain range and keeps the joint structure stable. The proposed robotic hand has a similar ligament cable added to inhibit the reverse-directional pitch motion of a joint and to keep the joint safe, as shown in Fig. 3. As an example, Fig. 4 shows the kinematic range of the middle finger. The inverse kinematics of the cable length can be obtained as follows: a point vector,  $P_i$ , of a hole on a joint knuckle is described in the base coordinates at the origin of a finger as

$$P_i^b = T_i \cdot P_i. \quad (1)$$

where  $T_i$  denotes the transformation matrix from the base coordinate to the  $i^{th}$  joint coordinates and  $P_i^b$  is the representation of  $P_i$  in the base coordinates. The transformation matrix,  $T_i$  is a function of the joint angles,  $\theta$  and  $\varphi$ . The total cable length to

TABLE III  
COMPARISON OF ROBOTIC HANDS

Robot hand	Number of fingers	Total weight (kg)	Degree of freedom	Number of actuators	Size	Contact force (N)	Under-actuation	Thumb opposability	Adaptive grip
Proposed robot hand	5	0.9	20	15	Human hand sized	6	Tendon / spring	0.0494	Yes
Biomimetic hand [4]	5	0.9	21	10	Human hand sized	-	Tendon / pulley	-	Yes
KITECH -hand [13]	4	0.9	16	16	$358\text{mm} \times 195\text{mm} \times 25\text{mm}$	4	No	0.1241	No
Gifu hand III [21]	5	1.4	16	19	$251\text{mm} \times 190\text{mm} \times 41\text{mm}$	3	Four-bar linkage	0.0490	Yes
Graspar hand [22]	3	1.3	8	3	-	-	Idler-pulley	-	Yes

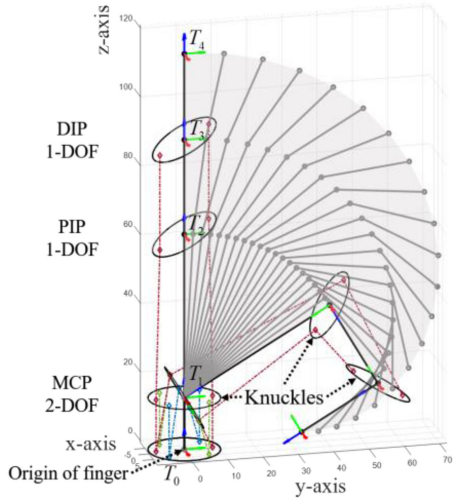


Fig. 4. Kinematic range of one finger.

the hole,  $P_i$  is obtained by

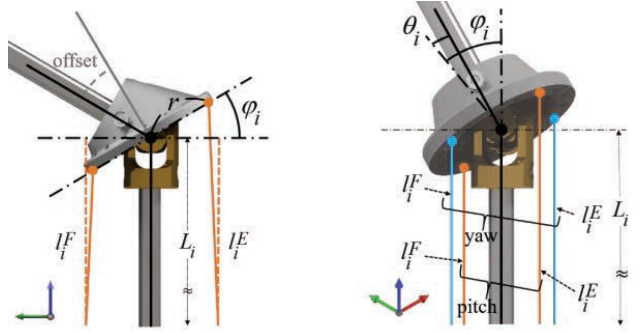
$$l_i = \sum_n^i \|P_n^b - P_{n-1}^b\| \quad (2)$$

It is possible to control a set of motors to achieve the desired cable lengths corresponding to the desired joint angles of fingers by using (2).

### III. DESIGN OF ROBOTIC HAND

#### A. Parallel Cable-Driven Joint With Single Motor

The flexion–extension functionality of the finger joints of the human hand are enabled by a set of muscles. Because a cable exerts only a pulling force, similar to the human muscle, at least two cables are required to obtain a motion of one DOF [23], [24]. Several studies on the cable-driven robotic hand used a cable-and-spring pair to enable the antagonistic motion at a joint in order to reduce the number of motors [17], [25], [26].



(a) One DOF joint for PIP and DIP      (b) Two DOF joint for MCP

Fig. 5. Parallel antagonistic cable-driven joints.

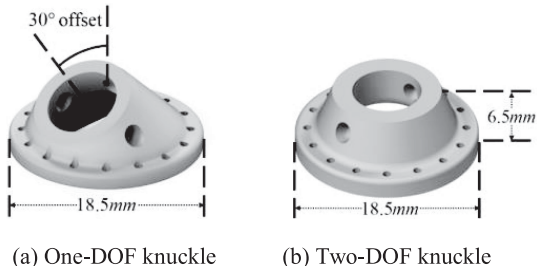


Fig. 6. Design of knuckle for universal joint.

In contrast, in this study, a pair of parallel cables winding in opposite directions on a motor is used.

Fig. 5 shows the joints of the proposed robotic hand with the antagonistic parallel cables. The design of the knuckle used in the joints is shown in Fig. 6; it has the application points of the pulling forces from the cables and provides the pathway holes of the cables for the next joints. The one-DOF knuckle for the PIP and the DIP joints has 30° offset angle on the vertical axis to enhance the working range of the joints, as shown in Fig. 6(a). To apply antagonistic actuation at a joint by a single motor, a bobbin with a pair of parallel cables winding in opposite directions, as shown in Fig. 7, is designed in this study. Because

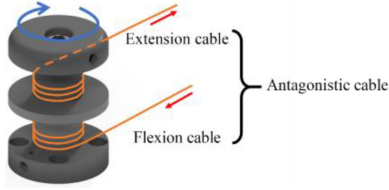


Fig. 7. Bobbin for antagonistic actuation by winding cables in opposite directions.

TABLE IV  
COMPONENTS OF THE HUMAN HAND AND THE ROBOTIC HAND

Human hand	Robotic hand
joint	universal joint (off-the-shelf)
bone	shaft (off-the-shelf)
muscle	cable and motor(off-the-shelf)
muscle attachment to bone	knuckle (3D printed)
muscle antagonism	bobbin (3D printed)

of the bobbin, only one motor needs to be used for the pair of antagonistic cables instead of using two independent motors for each cable. The knuckle and bobbin used in this study—shown in Figs. 6 and 7, respectively—are designed and produced by a tabletop 3D printer. The 3D printer has a nozzle with 0.4 mm diameter and 0.1 mm vertical resolution; it is the most popular fused deposition modeling type and uses the poly lactic acid filaments to produce the parts. Table IV shows the components of the robotic hand corresponding to those of the human hand.

The antagonistic actuation using the cable-driven parallel plates(knuckles) between joints in this study has advantages over the conventional robotic hand. The Graspar hand has the similar cable-driven antagonistic actuation [22]. However, the idler-pulley mechanism in the Graspar hand has only one DOF at a joint and has narrow working range. In comparison, the parallel plate mechanism in this study is able to achieves two DOFs at a joint and has relatively wider working range with simple structure. The cable-driven DART-hand [25], Spring hand [17], and 3D-printed hand [18] using the pulley with pin mechanism also have only one DOF at a joint.

It is noted that there is an inevitable difference in the length changes of the flexion and the extension cables when they are antagonistically actuated by a single motor. For example, the segments of the flexion and the extension cables between two adjacent joints have the lengths in (3) according to a joint angle  $\varphi_i$ :

$$\begin{aligned} l_i^F &= \sqrt{(L_i - r \sin \varphi_i)^2 + (r - r \cos \varphi_i)^2}, \\ l_i^E &= \sqrt{(L_i + r \sin \varphi_i)^2 + (r - r \cos \varphi_i)^2}. \end{aligned} \quad (3)$$

Here,  $l_i^F$  and  $l_i^E$  represent the lengths of the flexion and the extension cables, respectively;  $L_i$  denotes the phalange length and  $r$  is the radius of the knuckle (Fig. 5). In (3), the difference between the changes in the cable lengths according to the joint angle is not zero, i.e.,  $|\Delta l_i^F - \Delta l_i^E| \neq 0$  with respect to  $\Delta \varphi_i$ ; a cable can be slack over a certain joint angle. However, the

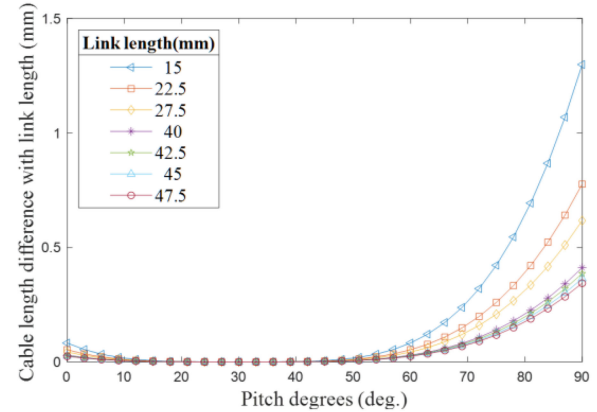


Fig. 8. Differences of cable lengths according to the joint angle.

TABLE V  
MOTOR CHARACTERISTICS

Appearance:	Input voltage	Recommended: 12V
	Stall current	1.4 A
	Stall torque	1.90 N·m
	No load speed	70 RPM
	Encoder resolution	4096 pulse/rotation
	Weight	65g

difference is approximately  $|\Delta l_i^F - \Delta l_i^E| \approx 0$  if  $L_i$  is larger than  $r$  enough in general. Fig. 8 shows the differences in the length changes of the antagonistic cables according to the joint angle of the robotic hand. The link lengths in the figure represent the phalange lengths in the proposed design as in Table II (b). As shown in Fig. 8, the cable length differences are small enough compared to the link length in entire range of the joint angle. More specifically for the worst case of the shortest phalange length,  $L_i = 15$  mm, the maximum error between two parallel cables is 1.3 mm that corresponds around 10° error of the joint angle.

### B. Motor

In this study, fifteen XC430-W240-Ts by ROBOTIS Co. are used as actuators of the robotic hand [27]. The ROBOTIS actuator includes a DC motor, a reduction gear, an optical encoder, a feedback controller, and a communication circuit in a compact package. The important characteristics of the motor are summarized in Table V. The main control program for the robotic hand is written in C++ running on PC and it communicates with the actuators through the half duplex USART multi-drop bus.

### C. Under-Actuation of PIP and DIP Joints

The PIP and the DIP joints of the human hand are under-actuated by a connecting tendon and exhibit dependent motion [28], [29]. Previous studies on robotic hands have implemented a coupled motion between the joints using a fixed mechanical

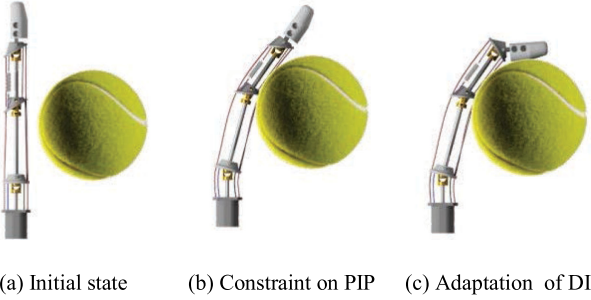


Fig. 9. Adaptive grasping.

linkage with loss of adaptive grasp [25], [30]. On the contrary, this study uses a compliant spring between the knuckles at the joints, as shown in Fig. 3. A pair of antagonistic cables passes through the pathway holes on the knuckle at the PIP joint and applies the actuation force to the knuckle at the DIP joint. Because of the connecting spring between the two joints, the motion of the DIP joint is transferred to the PIP joint. The PIP joint can thus adapt to the shape of an object being grasped by the under-actuation.

Fig. 9 shows the adaptive grasping of the PIP and the DIP joints. In free space, the actuation force on the DIP joint by the cables is transferred to the PIP joint by the spring and the two joints are bent simultaneously according to the force (Fig. 9(b)). When the PIP joint is constrained on contact with an object, the connecting spring extends and the DIP joint bends according to object's shape (Fig. 9(c)). The under-actuation helps to reduce the total number of motors in addition to enabling adaptive grasping.

#### D. Design for Thumb Opposability

The human hand has an opposable thumb that can flex and abduct against the other fingers. The opposability of the thumb serves an important role in cooperating with the other fingers to grasp and handle an object [1], [3], [13], [21]. The thumb opposability in (4) can be used as a performance index to evaluate the dexterity of an anthropomorphic robotic hand [13], [21]:

$$J = \frac{1}{d^3} \sum_{i=1}^4 w_i v_i \quad (4)$$

Here,  $d$  represents the length of the thumb,  $v_i$  denotes the common workspace between the thumb and the other fingers, and  $w_i$  is a weighting factor of each finger. The opposability depends on the thumb's orientation, as shown in Fig. 10, where every finger module except the thumb lies on the same palm plane and the thumb's direction points slightly downward. Table VI and Fig. 11 show the opposability of the robotic hand according to design of the thumb's orientation. The last row in Table VI is a common workspace between the thumb and corresponding finger normalized by the thumb length in Table II (b) with  $w_i = 1$  for all  $i$ . The thumb orientation of the robotic hand is designed at  $75^\circ$  to maximize the opposability while avoiding interference with the palm in this study. The common workspaces between

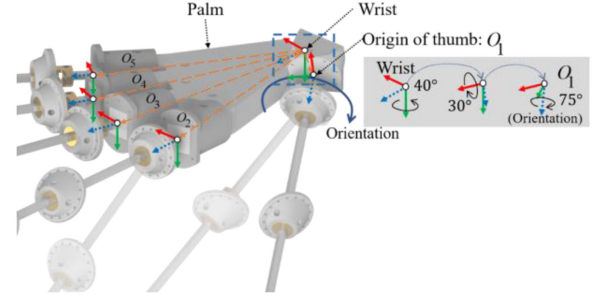


Fig. 10. Thumb origin for opposability design.

TABLE VI  
COMMON WORKSPACE BETWEEN THE THUMB AND THE OTHER FINGERS  
ACCORDING TO DESIGN OF THUMB'S ORIENTATION

Finger	Orientation of thumb			
	$65^\circ$	$70^\circ$	$75^\circ$	$80^\circ$
Index ( $cm^3$ )	125.4	128.4	131.1	133.1
Middle ( $cm^3$ )	152.1	153.5	154.3	154.4
Ring ( $cm^3$ )	150.1	151.0	151.4	151.5
Little ( $cm^3$ )	123.5	125.3	126.3	126.5
<i>Opposability J (<math>\times 10^{-2}</math>)</i>	4.84	4.90	4.94	4.96

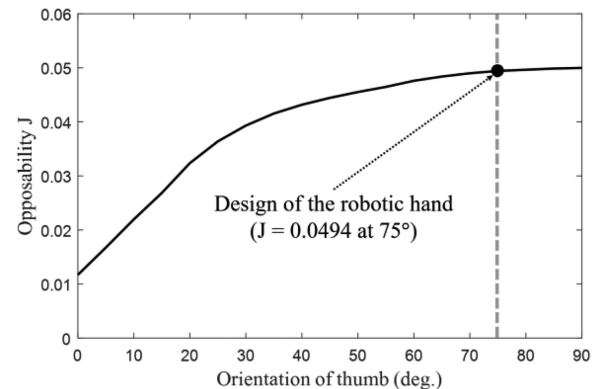


Fig. 11. Thumb's orientation for opposability.

the thumb and the other fingers at  $75^\circ$  orientation of thumb are shown in Fig. 12.

## IV. EXPERIMENT

### A. Performance of Finger

As a performance of the robotic hand, the contact forces are measured by a force-torque sensor as shown in Fig. 13. Fig. 14 is the graph of the index finger's contact force as an example. The maximum speeds of fingers in Table VII are calculated based on the angular speed of a motor, the radius of bobbin, and the change in the cable length according to a joint angle. The contact force and the speed of fingertips are tabulated in Table VII.

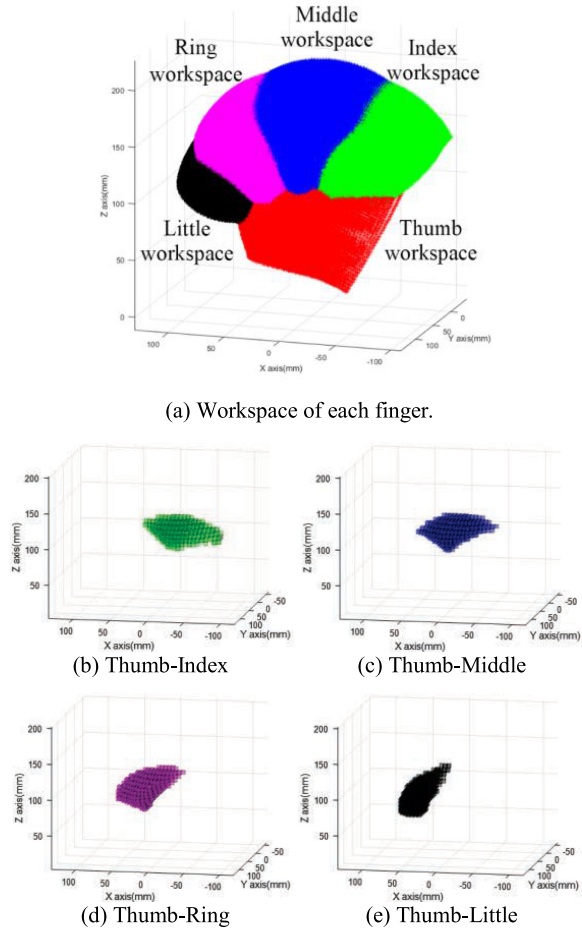


Fig. 12. Common workspaces between the thumb and the other fingers at 75° orientation of thumb.

TABLE VII  
PERFORMANCE OF FINGER

Finger	Thumb	Index	Middle	Ring	Little
Contact force (N)	6.15	6.24	6.41	6.01	5.83
Max speed (mm/s)	83.3	67.0	68.6	67.8	59.1

### B. Object Grasping

In the well-known Cutkosky's grasping taxonomy, there are two types of grasping: the precision grasp, which emphasizes dexterity and sensitivity, and the power grasp, which underlines the security and stability [31]. The grasping experiments of the proposed robotic hand are performed in accordance with the grasping taxonomy. Figs. 15 and 16 show the adaptive grasping of the robotic hand for various objects with the precision and the power grasps. Figs. 15(a) through 15(d) show the grasping for a pen, a cup, a Rubik's cube, and an aluminum disk which are an example of the tripod, the thumb-2 finger, the sphere, and the disk grasps suggested in [31]. Figs. 16(a) through 16(d) show the lateral pinch, the heavy wrap, the sphere, and the disk grasps in the power grasp category in [31]. Table VIII

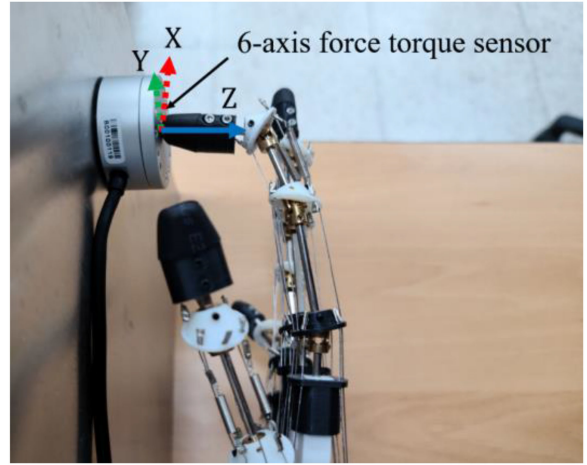


Fig. 13. Experimental setup for contact force measurement.

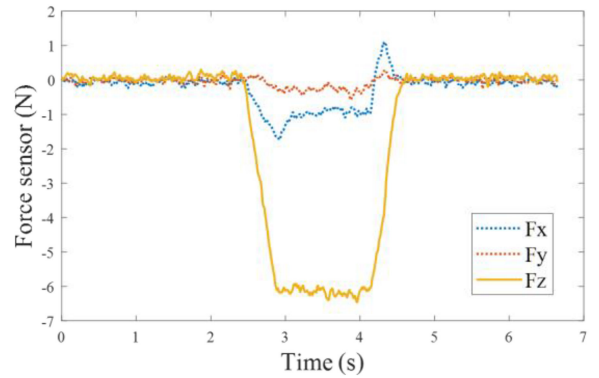


Fig. 14. Contact force of index finger.

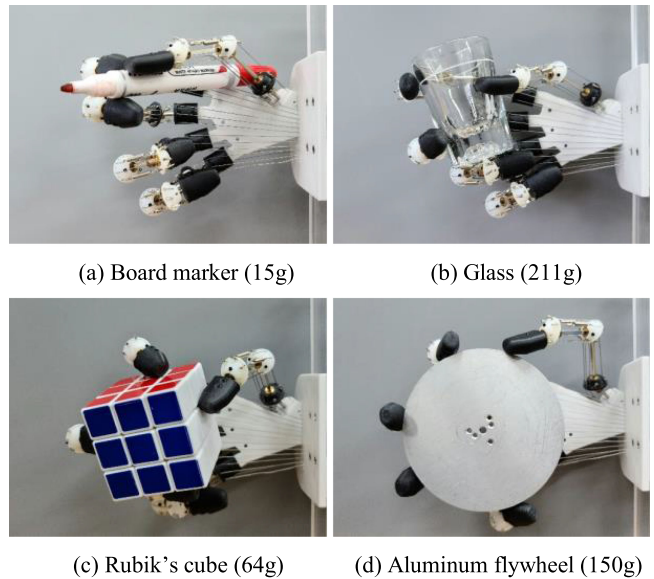


Fig. 15. Precision grasp.

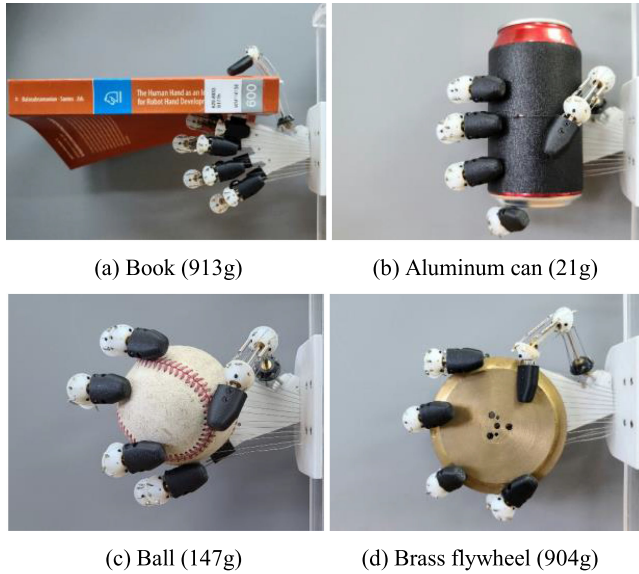


Fig. 16. Power grasp.

TABLE VIII  
GRASPING EXPERIMENTS IN ACCORDANCE WITH THE CUTKOSKY'S TAXONOMY

Grasping in Cutkosky's taxonomy			
Precision grasp		Power grasp	
Experiment	Taxonomy	Experiment	Taxonomy
Fig. 15 (a)	Tripod	Fig. 16 (a)	Lateral pinch
Fig. 15 (b)	Thumb-2 finger	Fig. 16 (b)	Heavy wrap
Fig. 15 (c)	Sphere	Fig. 16 (c)	Sphere
Fig. 15 (d)	Disk	Fig. 16 (d)	Disk

categorized the grasping experiments of the proposed robotic hand in accordance with the grasping taxonomy.

In case of the precision grasping, the contact surface between the robotic hand and the object exists on a fingertip. On the other hand, in case of the power grasping, the contact can occur on a cable according to the shape of an object as the hand is being actuated. The contact on a cable may cause instability and unintentional motion to the object in the middle of the grasping. At the final stage of the grasping, the target object is held by the knuckle joints and the fingertips and the stable grasping is achieved.

In the experiments, the roles of the opposable thumb are observed; the opposable thumb exhibits motion in a direction different from those of the other fingers, thereby preventing an object from skewing to one side and enabling safe object holding.

### C. Free-Space Motion

Figs. 17 through 19 show the free-space motions of the robotic hand. A motion sequence of “thumb up” by the robotic hand is shown in Fig. 17. Playing the rock-paper-scissors game and handshaking with the human hand are shown in Figs. 18 and 19. Table VII summarizes the linear velocity and contact force of the fingertip of the robotic hand. A short video clip of the robotic hand’s motion can be found in [32].

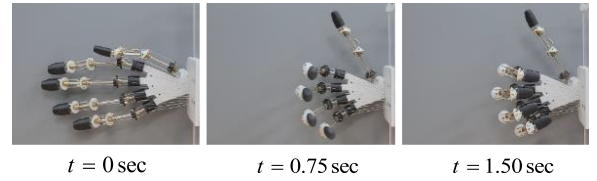


Fig. 17. Free-space motion: Thumbs up.

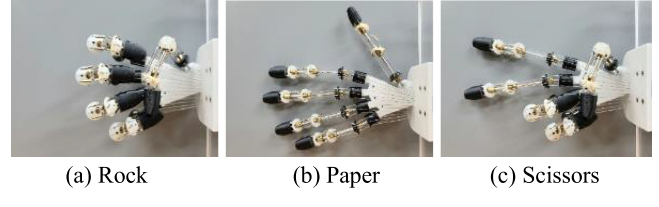


Fig. 18. Free-space motion: Rock-paper-scissors game.

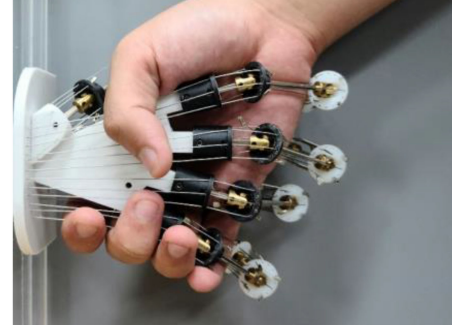


Fig. 19. Free-space motion: Handshaking.

## V. CONCLUSION

The conventional robotic hands used only one motor for each finger with fixed mechanical linkage at the cost of dexterity, or three or four motors deployed at each joint of a finger, resulting in a complex structure lacking power. This letter presents a novel anthropomorphic robotic hand that has a structure similar to those of a human hand. The proposed robotic hand comprises the joints that are driven by parallel cables; it has a light-weight and the adaptive grasping capability according to object’s shape. The main features of the proposed robotic hand can be summarized as follows: 1) antagonistic actuation for a joint, achieved by parallel cables with a single motor, 2) under-actuation between the PIP and the DIP joints for adaptive grasping, and 3) cost-effective implementation owing to the use of off-the-shelf and 3D-printable components. The cable-driven parallel plate mechanism in this study has advantages to achieve the antagonistic actuation; two DOFs at a joint and wide working range with simple structure. Experimental results validate the performances of the robotic hand, including its natural motion as well as the precision and the power grasping capabilities.

As the proposed design of the robotic hand used the parallel cables for the antagonistic actuation, there is a possibility of

force feedback control utilizing the cable tension and the corresponding change in the motor current without additional force sensors, which is under study.

#### ACKNOWLEDGMENT

The authors would like to thank Hyeonju Keum, Taewook Kim, and Donghyun Lee for their help in experiments.

#### REFERENCES

- [1] R. Balasubramanian and V. Santos, *The Human Hand as an Inspiration for Robot Hand Development*, Berlin, Germany: Springer, 2014.
- [2] J. Belter, J. Segil, A. Dollar, and R. Weir, "Mechanical design and performance specifications of anthropomorphic prosthetic hands: A review," *J. Rehabil. Res. Develop.*, vol. 50, no. 5, 2013, pp. 599–618.
- [3] B. G. Rutter, "The human hand," *Innov.: Hand*, Herndon, America, vol. 34, no. 1, May, 2015.
- [4] Z. Shu and E. Todorov, "Design of a highly biomimetic anthropomorphic robotic hand towards artificial limb regeneration," in *Proc. IEEE Int. Conf. Robot. Automat.*, pp. 16–21, 2016.
- [5] A. Deshpande *et al.*, "Mechanisms of the anatomically correct testbed hand," *IEEE/ASME Trans. Mechatronics*, vol. 18, no. 1, pp. 238–250, Feb. 2013.
- [6] C. Piazza, G. Grioli, M. Catalano, and A. Bicchi, "A century of robotic hands," *Annu. Rev. Control Robot. Auton. Syst.*, vol. 2, pp. 1–32, May 2019.
- [7] [Online] available: [https://www.ottobock.com/cps/rde/xchg/ob\\_us\\_en/hs.xls/6952.html](https://www.ottobock.com/cps/rde/xchg/ob_us_en/hs.xls/6952.html)
- [8] [Online] available: [https://www.ottobock.com/cps/rde/xchg/ob\\_com\\_en/hs.xls/3652.html](https://www.ottobock.com/cps/rde/xchg/ob_com_en/hs.xls/3652.html)
- [9] O. Bock, *Michelangelo Operation Manual*, Duderstadt, Germany: Otto Bock, 2012.
- [10] [Online] available: <https://handprothese.de/vincent-hand/>
- [11] [Online] available: <https://www.touchbionics.com/>
- [12] [Online] available: <https://rslstepper.com/>
- [13] D. Lee, J. Park, S. Park, M. Baeg, and J. Bae, "KITECH-Hand: A highly dexterous and modularized robotic hand," *IEEE/ASME Trans. Mechatronics*, vol. 22, no. 2, pp. 876–887, Apr. 2017.
- [14] G. Lum, S. Mustafa, H. Lim, W. Lim, G. Yand, and S. Yeo, "Design and motion control of a cable-driven dexterous robotic arm," in *Proc. IEEE Conf. Sustain. Utilization Develop. Eng. Technol.*, 2010, pp. 106–111.
- [15] L. Tran, Z. Zhang, S. Yeo, Y. Sun, and G. Yang, "Control of a cable-driven 2-DOF joint module with a flexible backbone," in *Proc. IEEE Conf. Sustain. Utilization Develop. Eng. Technol.*, 2011, pp. 150–155.
- [16] A. Caffaz, G. Casalino, G. Cannata, G. Panin, and E. Massucco, "The DIST-Hand, an anthropomorphic, fully sensorized dexterous gripper," in *Proc. IEEE Int. Conf. Humanoid Robots*, Daejeon, Rep. of Korea, 2000, pp. 418–422.
- [17] M. Carrozza *et al.*, "The SPRING hand: Development of a self-adaptive prosthesis for restoring natural grasping," *Auton. Robots*, vol. 16, pp. 125–141, 2004.
- [18] L. Tian, N. Thalmann, D. Thalmann, and J. Zheng, "The making of a 3D-Printed, Cable-driven, single-model, lightweight humanoid robotic hand," *Front. Robot. AI*, vol. 4, p. 65, 2017.
- [19] D. Riet, R. Stopforth, G. Bright, and O. Diegel, "A low cost design of a 3D printed multi-fingered myoelectric prosthetic hand," *Mechatronics: Princ., Tech. Apps.*, pp. 85–117, 2015.
- [20] R. Mio, B. Villegas, L. Ccorimanya, K. Flores, G. Salazar, and D. Elias, "Development and assessment of a powered 3D-printed prosthetic hand for transmetacarpal amputees," in *Proc. Int. Conf. Control, Automat. Robot.*, 2017, pp. 85–90.
- [21] T. Moura, H. Kawasaki, K. Yoshikawa, J. Takai, and S. Ito, "Anthropomorphic robot hand: Gifu hand III," in *Proc. Int. Conf. Autonomic Auton. Syst.*, 2002, pp. 1288–1293.
- [22] J. Chrisman, C. Kanjia, and I. Zeid, "Graspar: A flexible, easily controllable robotic hand," *IEEE Robot. Automat. Mag.*, vol. 3, no. 2, pp. 32–38, Jun. 1996.
- [23] A. Ming and T. Higuchi, "Study on multiple degree-of-freedom positioning mechanism using wires (part 1)," *Int. J. Jpn. Soc. Precis. Eng.*, vol. 28, no. 2, pp. 131–138, 1994.
- [24] R. Roberts, T. Graham, and T. Lippitt, "On the inverse kinematics, statics, and fault tolerance of cable-suspended robots," *J. Robotic Syst.*, vol. 15, pp. 581–597, 1998.
- [25] N. Thayer and S. Priya, "Design of implementation of a dexterous anthropomorphic robotic typing (DART) hand," *Smart Mater. Structures*, vol. 20, no. 3, 2011.
- [26] M. Cheng, L. Jiang, F. Ni, S. fan, Y. Liu, and H. Liu, "Design of a highly integrated underactuated finger towards prosthetic hand," in *Proc. IEEE Int. Conf. Adv. Intell. Mechatronics*, pp. 1035–1040, 2017.
- [27] [Online] available: <https://emanual.robotis.com/docs/en/dxl/x/xc430-w240/>
- [28] J. Michael and J. Bowker, "Partial-hand amputations: Surgical principles," in *Atlas of Amputations and Limb Deficiencies: Surgical, Prosthetic, and Rehabilitation Principles*, St. Louis (MO): Mosby Year Book, 2004.
- [29] H. Schmidt and U. Lanz, *Surgical Anatomy of the Hand*. Stuttgart: Thieme, 2004.
- [30] N. Wang, K. Lao, and X. Zhang, "Design and myoelectric control of an anthropomorphic prosthetic hand," *J. Bionic Eng.*, vol. 14, pp. 47–59, 2017.
- [31] M. Cutkosky, "On grasp choice, grasp models, and the design of hands for manufacturing tasks," *IEEE Trans. Robot. Automat.*, vol. 5, pp. 269–279, Jun. 1989.
- [32] [Online] available: <https://youtu.be/GzXvqFWgIs4>